RSC Advances

PAPER

View Article Online
View Journal | View Issue

Cite this: *RSC Adv.*, 2026, **16**, 4170

New multitarget antidiabetic potential agents based on sulfaguanidine: design, synthesis, and biological evaluation

Mohammed Salah Ayoup,*[a] Asmaa E. Kassab,[b] Amr Sonousi,[bc] Shaimaa E. Eldaly,[d] Jawaher Y. Al Nawah,[a] Hamida Abdel-Hamid,[d] Doaa A. Ghareeb,[efg] Samah Ashraf[e] and Manar Ahmed Fouad*[d]

Diabetes-related morbidity and mortality rates are high, making type 2 diabetes (T2DM) a serious issue at an alarming rate. This work focused on the design and synthesis of a series of new sulfaguanidine derivatives connected through a hydrazine linker to five-membered heterocycles. All synthesized derivatives were screened for *in vitro* α-amylase, α-glucosidase, and glucose uptake activities. Interestingly, all the synthesized sulfaguanidine derivatives exhibited significant α-glucosidase and α-amylase inhibitory potentials that were more potent than acarbose. Sulfaguanidine derivative **10** (IC_{50} = 0.39 μM) exhibited the most potent α-glucosidase inhibition among all the synthesized derivatives, which was 7.43-fold more potent than acarbose. Compound **4** (IC_{50} = 0.33 μM) was the most potent derivative, exhibiting the strongest α-amylase inhibition and a glucose uptake activity, 1.20- to 1.92-fold higher than that of berberine. The prominent interactions with the α-amylase and α-glucosidase active sites can be used to computationally rationalize the significant *in vitro* inhibitory activity of the synthesized sulfaguanidine derivatives against both enzymes. This study reveals that sulfaguanidine-conjugated pyrazole or oxazole derivatives are prospective multitarget therapeutic candidates that can be employed for the treatment of T2DM, which is characterized by complicated etiologies.

Received 19th November 2025
Accepted 5th January 2026

DOI: 10.1039/d5ra08959j

rsc.li/rsc-advances

1. Introduction

Diabetes mellitus (DM) is a chronic, serious metabolic disease that is characterized by an impaired insulin response and difficulty using glucose for energy, which causes blood sugar levels to rise.[1] Acute consequences such as diabetic ketoacidosis and nonketotic hyperosmolar coma are caused by uncontrolled diabetes. Numerous tissue damage conditions that lead to stroke, foot ulcers, weakened immunity, renal failure, cardiovascular disease, and eye damage are examples of chronic consequences.[1] DM represents a pressing worldwide health crisis. Current estimates from the International Diabetes Federation (IDF) indicate that DM affects more than 537 million people aged 20–79, with projections suggesting an increase to 783 million by 2045. The substantial scale of this disease is further highlighted by the associated global healthcare costs, which reached nearly USD 966 billion in 2021.[2,3] Type 2 DM (T2DM), usually referred to as non-insulin-dependent diabetes mellitus, accounts for 90% of all cases of diabetes worldwide.[4,5] In developing countries, T2DM is a significant problem that is becoming increasingly prevalent, with high rates of diabetes-related morbidity and mortality. According to predictions, the number of people with T2DM will continue to rise over the next 20 years, with over 70% of those patients living in developing countries, predominantly among those aged 45 to 64.[6] Despite the notion that older age is a risk factor for T2DM, rising childhood obesity rates have made the disease more prevalent in children, teenagers, and young adults, which is a major emerging public health issue of substantial proportions.[7]

Controlling blood glucose levels early on reduces the risk of diabetic complications that lower the quality of life. The enzyme α-amylase breaks down polysaccharides to yield disaccharides and oligosaccharides, which are then broken down by the enzyme α-glucosidase to produce monosaccharide units.[8] The activity of these enzymes is targeted by α-amylase and α-

[a]*Department of Chemistry, College of Science, King Faisal University, Al-Ahsa 31982, Saudi Arabia. E-mail: mayoup@kfu.edu.sa*
[b]*Department of Pharmaceutical Organic Chemistry, Faculty of Pharmacy, Cairo University, Kasr El-Aini Street, P.O. Box 11562, Cairo, Egypt*
[c]*Department of Pharmaceutical Sciences, College of Pharmacy, Gulf Medical University, Ajman, United Arab Emirates*
[d]*Department of Chemistry, Faculty of Science, Alexandria University, P.O. Box 426, Alexandria 21321, Egypt. E-mail: manar.ahmed@alexu.edu.eg*
[e]*Bio-screening and Preclinical Trial Lab, Biochemistry Department, Faculty of Science, Alexandria University, Alexandria, Egypt*
[f]*Center of Excellence for Drug Preclinical Studies (CE-DPS), Pharmaceutical and Fermentation Industry Development Center, City of Scientific Research & Technological Applications (SRTA-city), New Borg El Arab, Alexandria, Egypt*
[g]*Research Projects Unit, Pharos University in Alexandria, Canal El Mahmoudia Street, Beside Green Plaza Complex, 21648, Alexandria, Egypt*

glucosidase inhibitors like acarbose and miglitol, which can inhibit the digestion of carbohydrates, causing a delay in the absorption of glucose and resulting in decreased blood sugar levels. These drugs frequently have adverse side effects, including flatulence, bloating, diarrhea, and abdominal pain.[9–12] Furthermore, these drugs have been shown to lose their effectiveness over time, so there is a great need for new and more effective α-amylase and α-glucosidase inhibitors.

Numerous drug alternatives are available to treat T2DM, including insulin secretagogues, like sulphonylureas and

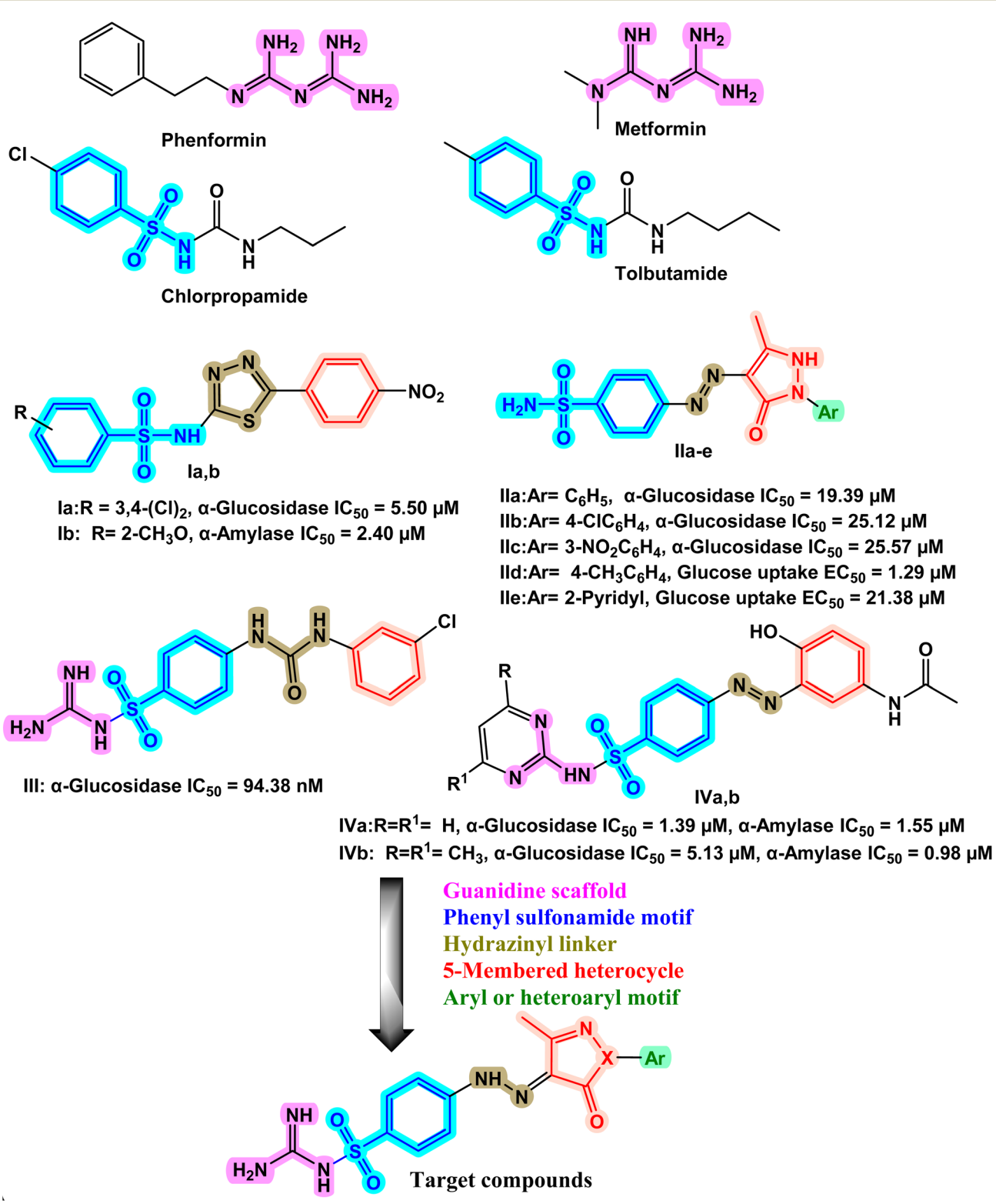

Fig. 1 Design strategy for the targeted sulfaguanidine derivatives.

meglitinides, which enhance insulin secretion from pancreatic β-cells, glucose-lowering medications that improve glucose absorption, and inhibit the synthesis of glucose in the liver, and biguanides, which lower blood glucose primarily by decreasing hepatic glucose production.[13] None of the antidiabetic drugs used to treat hyperglycemia can prevent or reverse the progression of the disease, and some of them may even have serious side effects and contribute to comorbidities.[14] This necessitates the continued search to develop novel multitarget therapeutic agents for glycemic control.

Metformin[15,16] and phenformin[17] (Fig. 1) are biguanide antidiabetic drugs used to lower blood glucose concentrations in patients with T2DM. Chlorpropamide and tolbutamide (Fig. 1) are among the phenyl sulfonylureas that are extensively used for the treatment of T2DM.[18] A recent study reported the α-glucosidase and α-amylase inhibitory potentials of thiadiazole-containing sulfonamide derivatives **Ia** and **Ib** (Fig. 1).[19] Our research group developed sulfonamide derivatives **IIa–e** (Fig. 1) as multitarget antidiabetic agents that exhibited excellent inhibitory potential against α-glucosidase; additionally, they exhibited significant glucose uptake activity.[20] Various sulfaguanidine-based compounds have been reported with potent antidiabetic activity, exerting their potential *via* α-amylase and α-glucosidase inhibition, such as compounds **III** (ref. 21) and **IVa,b** (ref. 22) (Fig. 1).

According to recent trends in medicinal chemistry research, molecular hybridization, which is based on combining two or more pharmacophoric moieties of different biologically active drug candidates to create a new hybrid molecule with higher effectiveness and affinity for improved binding interactions and better pocket packing of inhibitors to the receptors, is increasingly attractive and widely accepted approach for drug synthesis.[23]

In the search for new antidiabetic agents, the choice of core chemical structures is of great importance. Nitrogen-containing heterocycles are exceptionally significant in medicinal chemistry, forming the backbone of countless drugs.[24–27] Their versatility and stability make them ideal scaffolds for building bioactive molecules. Moreover, the sulfaguanidine moiety is a highly valuable pharmacophore, prized for its strong hydrogen-bonding capacity and structural rigidity.[28] The combination of these two important chemical features, a robust *N*-heterocyclic core and the versatile sulfaguanidine unit, provides a powerful and rational approach for the synthesis of new chemical entities with high potential for antidiabetic activity.

Inspired by the information mentioned earlier and the ongoing efforts of our research team to create novel heterocyclic compounds with potential antidiabetic activity, we describe the synthesis of new sulfaguanidine derivatives that incorporate essential pharmacophoric features of reported potent antidiabetic drugs and drug candidates (Fig. 1). Firstly, the privileged guanidine scaffold was used to design the targeted compounds. The guanidine motif can bind to anions using H-bonds, charge pairing, and cation–π interactions, enabling it to form non-covalent interactions with proteins and other molecular targets.[29] The second strategy involved the incorporation of the phenyl sulfonamide motif. To share as H-bond acceptors and/or donors with amino acids in the active sites of α-glucosidase and α-amylase enzymes, a hydrazinyl linker was incorporated in the third strategy. Within the fourth strategy, a five-membered heterocycle (pyrazole or oxazole) was grafted. In the fifth strategy, different hydrophobic aromatic moieties were grafted to the pyrazole motif. The substitution design of these hydrophobic moieties ensured a range of electronic and lipophilic environments that could impact the target compounds' activity. The design of the synthesized sulfaguanidine derivatives ensures their ability to act on multiple diabetes-related targets, including α-glucosidase, α-amylase, and glucose uptake mechanisms. Targeting these complementary pathways may provide synergistic control of hyperglycemia and lead to improved therapeutic efficacy in T2DM. All the synthesized derivatives were assessed for their ability to inhibit α-glucosidase and α-amylase *in vitro* as well as their effect on yeast cells' uptake of glucose. They were subjected to docking simulations on the α-glucosidase protein (PDB: 2QMJ) and α-amylase (PDB: 1XCW) both complexed with acarbose.

2. Results and discussion

2.1. Chemistry

Continuing our work to explore new medical applications for sulfa drug derivatives, herein, we prepared a series of hybrid sulfaguanidine/pyrazole or isoxazole derivatives. The functionalization protocol of the sulfaguanidine (Scheme 1) was accomplished initially by diazotization of the sulfaguanidine (**1**) using an acidified $NaNO_2$ protocol to form the diazonium salt **2**. Then, coupling of **2** with ethyl acetoacetate as the carbanion source at 0 °C to afford the corresponding ethyl (*E*)-2-(2-(4-(*N*-carbamimidoylsulfamoyl)phenyl)hydrazono)-3-oxobutanoate (**3**). The structure of **3** was confirmed by spectroscopic analysis. For instance, the characteristic guanidine group $H_2NC(NH)NHSO_2$ showed strong, broad absorption bands in the IR spectrum at 3464, 3415, 3364, 3328, and 3225 cm^{-1}, while the ^1H NMR spectrum showed a strong, broad signal at 6.69 ppm corresponding to the four protons of the sulfaguanidine moiety $\mathbf{H_2}NC(N\mathbf{H})N\mathbf{H}SO_2$. The IR spectrum also showed a strong band at 1666 cm^{-1} for the conjugated (C=N) group. Moreover, the ^1H NMR spectrum of **3** showed a singlet signal in the downfield, assigned to an NH at δ_H: 11.57 ppm. Furthermore, the protons of the aliphatic protons showed three sets of signals in the upfield region at δ_H 4.32, 2.40, and 1.28 ppm, revealing the presence of $OC\mathbf{H_2}$, $COC\mathbf{H_3}$, and $C\mathbf{H_3}$, respectively. Also, the ^{13}C NMR spectrum confirmed the presence of the acetyl and ester groups, where two nonhomotopic carbonyls at δ_C: 193.8 and 162.4 ppm, respectively, were present alongside the aliphatic carbons at δ_C: 61.3, 25.3, and 13.9 ppm.

Cyclization of **3** with aryl hydrazine derivatives, namely phenylhydrazine, *o*-fluorophenylhydrazine, *m*-fluorophenylhydrazine, *p*-chlorophenylhydrazine, *p*-nitrophenylhydrazine, 4-hydrazinobenzene sulfonamide, 2-pyridylhydrazine, or *p*-tolylhydrazine, afforded the corresponding sulfaguanidine/pyrazole hybrids (**4–11**). The ^{13}C NMR of the hybrids **4–11** showed the carbonyl carbon of the pyrazolone ring

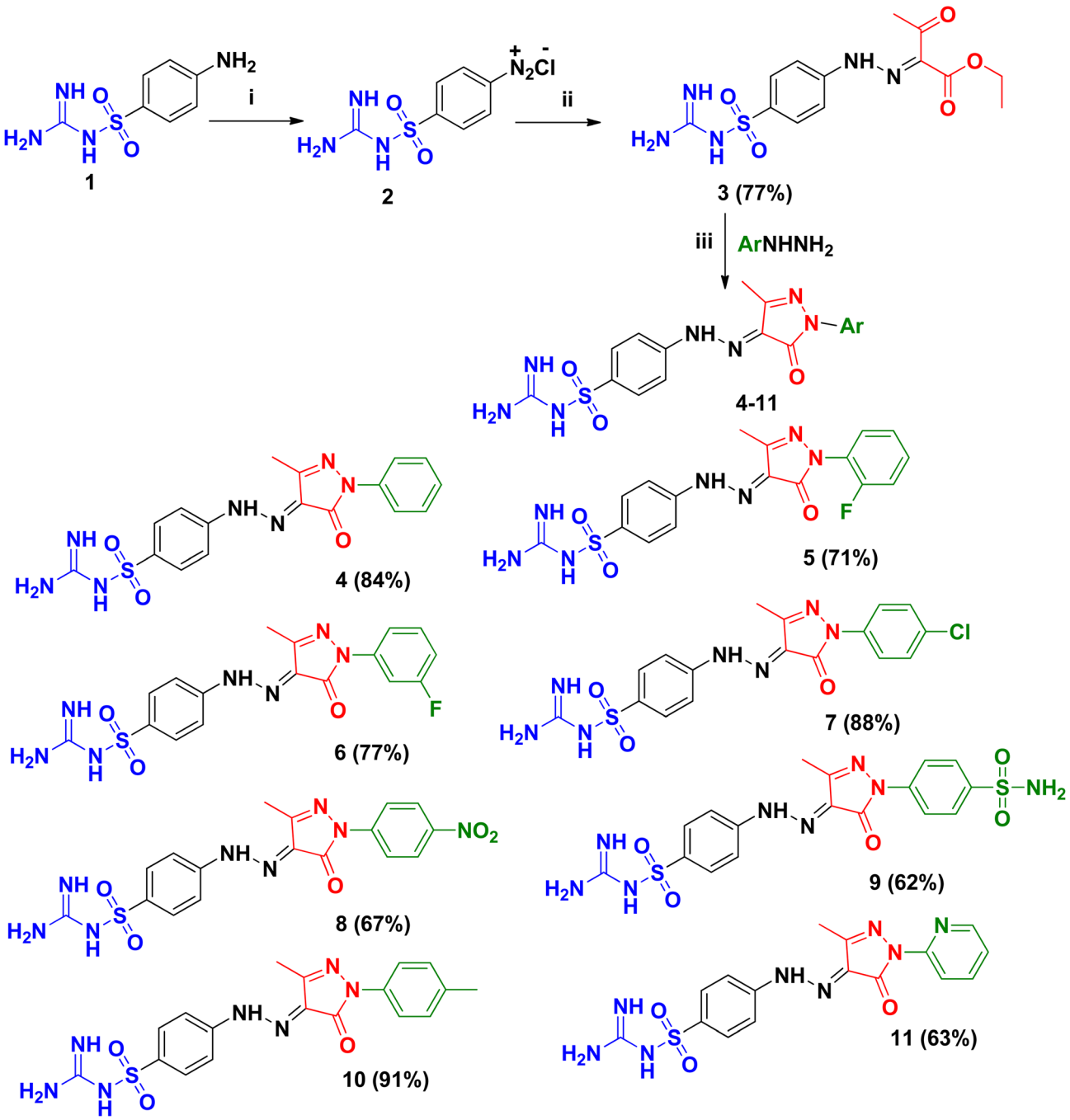

Reagents and conditioins:
i) sodium nitrite, glacial acetic acid, water, 0°C
ii) ethyl acetoacetate, sodium acetate, ethanol, water, 0-5°C, stir 4h.
iii) ethanol, reflux 6h.

Scheme 1 Synthetic pathway and reagents for preparing target compounds 2–11.

at the range δ_C: 155.9–162.1 ppm and the C=N of the sulfaguanidine moiety $H_2NC(NH)NHSO_2$ resonating at 158.0–152 ppm. The CH_3 group of the pyrazolone moiety resonated at δ_C: 10.1–11.8 ppm. Moreover, the characteristic signal of the C–F bond of the aryl pyrazole **5** and **6** appeared at δ_C: 155.9, 162.6 ppm, respectively, with $^1J_{CF}$ = 249.5 and 240.8 Hz, respectively.

Sulfaguanidine hydrazone/isoxazole or pyrazolone hybrids **12** and **13** (Scheme 2) were synthesized by refluxing compound **3** with ethanolic hydroxylamine or hydrazine, respectively. The IR

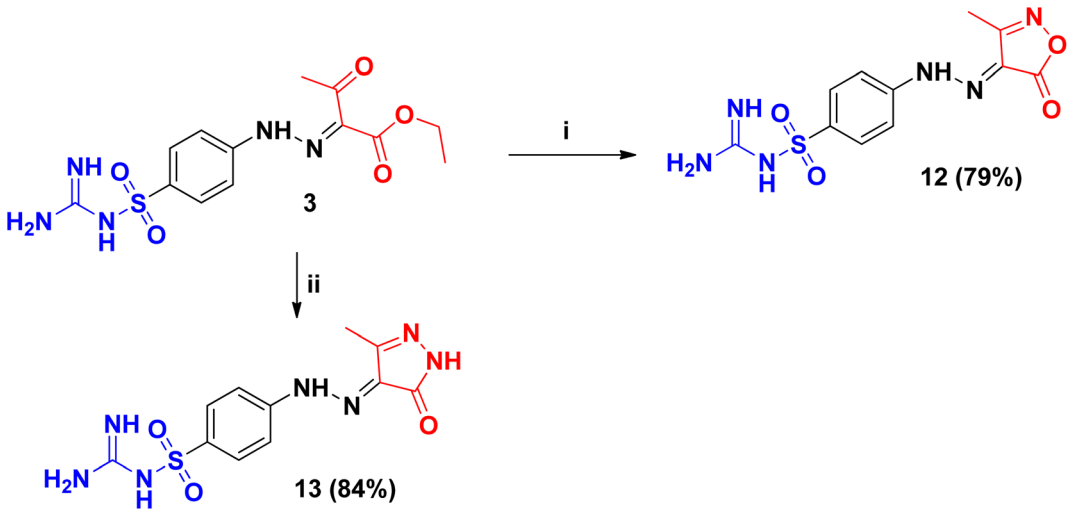

Scheme 2 Synthetic pathways and reagents for the preparation of target compounds **12** and **13**.

spectra of **12** and **13** showed a strong band attributed to C=O at ν_{max} 1718 and 1672 cm^{-1}, respectively. The ^{1}HNMR of **12** and **13** showed broad signals corresponding to N**H** at δ_H: 12.77 and 11.61 ppm, respectively, beside the remarkable signals corresponding to sulfaguanidine moiety **H**$_2$NC(N**H**)N**H**SO$_2$ at δ_H: 6.72 and 6.70 ppm, respectively. Moreover, the ^{13}CNMR spectrum confirmed the presence of **C**=O of the heterocyclic rings in compounds **12** and **13**, which was indicated by a signal at δ_C: 162.1 and 160.6 ppm, respectively.

2.2. α-Glucosidase inhibitory activity and structural activity relationship

The *in vitro* α-glucosidase inhibition activities of synthesized sulfaguanidine derivatives were assessed by comparing their half maximum inhibitory concentration (IC_{50}) values to acarbose, a reference antidiabetic drug. Table 1 provides an overview of the results. The results showed that all the synthesized sulfaguanidine derivatives with IC_{50} values in the range of 0.39 to 1.61 μM exhibited excellent α-glucosidase inhibitory potential that was 1.80 to 7.43 times more potent than that of acarbose (IC_{50} = 2.90 μM). The structure–activity relationship (SAR) was investigated through cyclization of the oxobutanoate moiety of the parent sulfaguanidine derivative **3** into oxazole or pyrazole moieties. The pyrazole moiety was substituted in some derivatives with phenyl or pyridyl motifs (Fig. 2). The parent sulfaguanidine derivative **3** exhibited excellent inhibitory potency, with an IC_{50} value of 0.44 μM. Cyclization of the oxobutanoate moiety to pyrazole incorporating unsubstituted phenyl (**4**) resulted in a marked decrease in the α-glucosidase inhibition (IC_{50} = 1.58 μM). Substitutions on the phenyl ring or incorporation of a pyridyl moiety (compounds **5–11**) greatly enhanced the α-glucosidase inhibitory activity. Sulfaguanidine derivative **10** (IC_{50} = 0.39 μM) with the phenyl moiety substituted with a methyl group exhibited the most potent activity among all the synthesized derivatives, indicating the positive impact of the electron-donating group on the α-glucosidase inhibition. Among the electron-withdrawing substituents on the phenyl moiety, the fluorine atom (compounds **5** and **6**) revealed the most prominent activity, with IC_{50} values of 0.57 and 0.45 μM, respectively. Replacement with chlorine in compound **7** (IC_{50} = 1.26 μM), a nitro group in compound **8** (IC_{50} = 0.61 μM), or a sulfonamide group in compound **9** (IC_{50} = 0.83 μM) resulted in a decrease in the activity. Incorporation of the pyridyl scaffold on the pyrazole moiety in compound **11** was highly tolerated for the α-glucosidase inhibitory activity, with an IC_{50} value of 0.59 μM. An interesting observation is that the cyclization of the oxobutanoate moiety of the parent

Table 1 Biological evaluation results

	α-Glucosidase	α-Amylase	Glucose uptake
Compound	[a]IC_{50} (μM ± SD)	[a]IC_{50} (μM ± SD)	[a]EC_{50} (μM ± SD)
3	0.44 ± 0.08	0.35 ± 0.02	26.55 ± 0.12
4	**1.58 ± 0.16**	**0.33 ± 0.04**	56.87 ± 0.27
5	**0.57 ± 0.11**	**0.80 ± 0.09**	87.77 ± 0.19
6	**0.45 ± 0.09**	**0.48 ± 0.06**	88.19 ± 0.06
7	**1.26 ± 0.03**	**0.85 ± 0.12**	50.11 ± 0.22
8	**0.61 ± 0.17**	**0.73 ± 0.1**	**30.02 ± 0.13**
9	**0.83 ± 0.11**	**0.57 ± 0.04**	**33.81 ± 0.09**
10	**0.39 ± 0.02**	**1.13 ± 0.14**	83.89 ± 0.14
11	**0.59 ± 0.08**	**0.54 ± 0.07**	117.22 ± 0.14
12	**1.09 ± 0.03**	**0.61 ± 0.08**	**21.14 ± 0.08**
13	**1.61 ± 0.14**	**1.33 ± 0.12**	57.30 ± 0.17
Acarbose	2.90 ± 0.51	1.72 ± 0.51	—
Berberine	—	—	40.70 ± 3.12

[a] All values are expressed as the mean of three replicates.

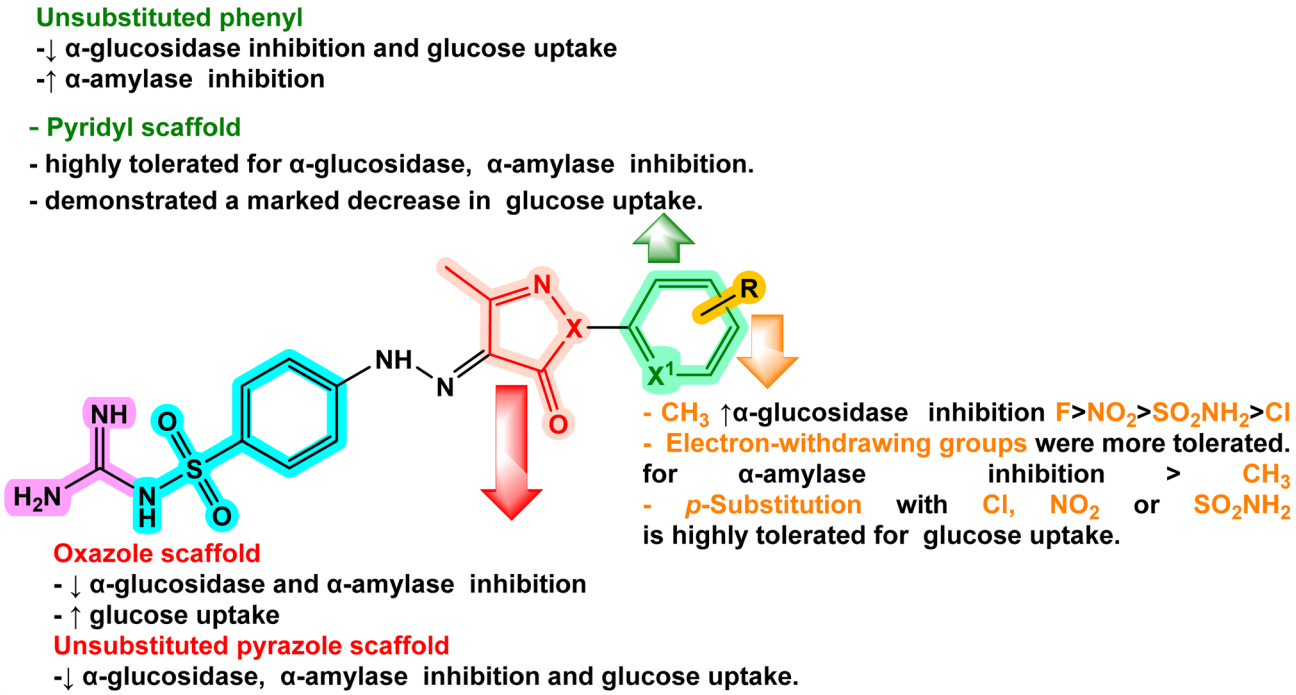

Fig. 2 Structure–activity relationship (SAR) of the synthesized sulfaguanidine derivatives.

sulfaguanidine derivative into oxazole in compound **12** (IC_{50} = 1.09 μM) or the unsubstituted pyrazole moiety in compound **13** (IC_{50} = 1.61 μM) reduced the α-glucosidase inhibitory activity.

The bold text indicates the more potent compounds than the reference standard.

2.3. α-Amylase inhibitory activity and structural activity relationship

The IC_{50} values of all synthesized compounds were calculated and compared to acarbose to assess their inhibitory potentials against α-amylase (Table 1). The results showed that all the synthesized sulfaguanidine derivatives with IC_{50} values in the range of 0.33 to 1.33 μM exhibited excellent α-amylase inhibitory potential that was 1.29 to 5.21 times more potent than that of acarbose (IC_{50} = 1.72 μM). With an IC_{50} value of 0.35 μM, the parent sulfaguanidine derivative **3** demonstrated excellent α-amylase inhibitory efficacy. Cyclization of the oxobutanoate moiety to pyrazole, incorporating an unsubstituted phenyl in compound **4** (IC_{50} = 0.33 μM) resulted in the most potent α-amylase inhibitory potential among the synthesized sulfaguanidine derivatives. Substitution of the phenyl ring with electron-withdrawing groups in compounds **5–9**, with IC_{50} values in the range of 0.48–0.85 μM, slightly reduced the activity. Substitution of the phenyl ring with the electron-donating methyl group in compound **10**, with an IC_{50} value of 1.13 μM, resulted in a decline in α-amylase inhibition. Grafting the pyridyl scaffold on the pyrazole moiety in the sulfaguanidine derivative **11** (IC_{50} = 0.54 μM) revealed a positive impact on the activity. Cyclization of the oxobutanoate moiety of the parent sulfaguanidine derivative into oxazole in compound **12** (IC_{50} = 0.61 μM) or an unsubstituted pyrazole moiety in compound **13** (IC_{50} = 1.33 μM) reduced the activity. It is worth mentioning that compound **13** exhibited the least potent α-amylase inhibitory activity among all the synthesized derivatives, revealing the positive impact of grafting hydrophobic aromatic moieties to the pyrazole motif on the α-amylase inhibitory potential of the synthesized sulfaguanidine derivatives (Fig. 2).

2.4. Glucose uptake assay and structural activity relationship

In vitro screening for the hypoglycemic action of drug candidates can be done using the yeast cells' uptake of glucose.[30] Yeast cells were exposed to glucose and various concentrations of the tested compounds for a predetermined period. The amount of glucose that remained after this time serves as an indication of how well the yeast cells absorbed the glucose. Each compound was tested at five different concentrations, and the EC_{50} values, representing the concentration of the compound at which 50% of glucose absorption occurs, were calculated for each compound. Higher antidiabetic action is indicated by a lower EC_{50} value (Table 1). All compounds showed an increase in glucose uptake with increased concentrations. The parent sulfaguanidine derivative **3** exhibited excellent glucose uptake activity, with an EC_{50} value of 26.55 μM, which was 1.53-fold more potent than the reference standard berberine (EC_{50} = 40.70 μM). Cyclization of the oxobutanoate moiety to the pyrazole scaffold incorporating a phenyl ring in compounds **4–10** (EC_{50} values in the range of 30.02–88.19 μM) resulted in decreased activity. Sulfaguanidine derivatives **8** (EC_{50} = 30.02 μM) and **9** (EC_{50} = 33.81 μM) incorporating *p*-nitro and *p*-sulfonamide groups were the most potent in this series, with potencies 1.35- and 1.20-fold greater than that of berberine,

Table 2 The docking scores of the target compounds

Compound	Docking score (PDB: 2QMJ) (kcal mol^{-1})	Interactions	Docking score (PDB: 1XCW) (kcal mol^{-1})	Interactions
3	−6.659	2HB (Asp443) HB (His600) HB (Asp542) Arene–H (Trp406)	−7.393	HB (His201) HB (His299) HB (Asp300) HB (Asp197) Arene–H (Leu162)
4	−6.641	HB (Asp542) HB (Met444) HB (His600) HB (Trp539) HB (Trp406) Arene–H (Met444)	−7.0595	HB (Glu233) HB (His305) HB (His201) Arene–H (Ile235) Arene–H (Ala307)
5	−6.400	HB (Asp443) 2HB (Met444) HB (Asp327) Arene–H (Trp406) Arene–H (Phe450)	−6.977	HB (Asp197) HB (His299) HB (Asp300) Arene–H (Leu162)
6	−6.220	HB (Asp443) 2HB (Met444) HB (Asp327) Arene–H (Trp406) Arene–H (Phe450)	−7.003	HB (His299) HB (Asp300) HB (Asp197) Arene–H (Leu162) Arene–H (Ile235) Arene–H (His201)
7	−6.665	HB (Met444) HB (Asp327) Arene–H (Phe575)	−7.088	HB (Asp300) HB (Glu233) HB (His201) Arene–H (Ile235) Arene–H (Ala307)
8	−7.254	HB (Asp327) HB (His600) HB (Asp542) HB (Trp406) Arene–H (Phe575)	−7.369	HB (His201) HB (Lys200) Arene–H (His101)
9	−6.863	HB (His600) HB (Asp443) HB (Met444) HB (Trp406) HB (Asn207)WB	−7.419	HB (Asp300) HB (Glu233) HB (His201) Arene–H (Ile235) Arene–H (Ala307)
10	−6.872	HB (Trp406) HB (His600) HB (Met444) Arene–H (Phe575)	−7.199	HB (Glu233) HB (His201) HB (His305) Arene–H (Ala307) Arene–H (Ile235)
11	−6.454	2HB (Asp443) HB (Met444) HB (His600)	−7.179	HB (His299) HB (Asp197) HB (Arg195) Arene–H (Ala307)
12	−6.631	HB (Asp542) HB (Met444)	−7.460	HB (Lys200) HB (His201) HB (Arg195) HB (Asp197) HB (His299) Arene–H (Ile235)
13	−6.696	HB (Asp327) HB (Asp443) 2HB (Met444) Arene–H (Trp406)	−6.799	HB (Lys200) HB (His201) HB (His299) Arene–H (Ile235) Arene–H (Trp58)
Acarbose	−7.8552	HB (Arg526) HB (Met444) HB (His600) HB (Asp203) HB (Asp542)	−8.249	HB (Lys200) HB (Arg195) HB (His201) HB (His101) HB (Asp197) HB (His299) HB (Arg195)

respectively. Compound **7**, incorporating a *p*-chloro group (EC_{50} = 50.11 μM), revealed glucose uptake activity comparable to berberine. These results indicated that the *para*-substitution of the phenyl ring with an electron-withdrawing group is more favorable for the activity. Grafting the pyridyl scaffold on the pyrazole moiety in the sulfaguanidine derivative **11** (EC_{50} = 117.22 μM) demonstrated a marked decrease in the activity. Cyclization of the oxobutanoate moiety of the parent sulfaguanidine derivative into oxazole in compound **12** (EC_{50} = 21.14 μM) revealed the most potent glucose uptake activity, which was 1.92-fold more potent than berberine; on the other hand, cyclization into the unsubstituted pyrazole moiety in compound **13** (EC_{50} = 57.30 μM) reduced the activity (Fig. 2).

2.5. Comparison with previous studies, novelty, and implications

A direct comparison with currently available antidiabetic drugs was conducted to further contextualize the therapeutic significance of the synthesized molecules. The reference standard for enzyme inhibition was acarbose, a clinically licensed α-glucosidase and α-amylase inhibitor; the reference drug for glucose uptake was berberine. Interestingly, all the synthesized sulfaguanidine derivatives showed better α-glucosidase inhibitory activity than acarbose (IC_{50} = 2.90 μM), with compound **10** showing the strongest inhibition (IC_{50} = 0.39 μM), representing a 7.43-fold increase in potency, while compound **3** (IC_{50} = 0.44 μM) showed a 6.59-fold enhancement. Several sulfaguanidine compounds demonstrated significantly increased α-amylase inhibition compared to acarbose (IC_{50} = 1.72 μM), especially compound **4** (IC_{50} = 0.33 μM), which was approximately 5.21 times more effective, whereas compound **3** showed a 4.91-fold increase in activity. Regarding glucose uptake, compound **12** (EC_{50} = 21.14 μM) enhanced glucose uptake by 1.92-fold compared to berberine (EC_{50} = 40.70 μM), while compounds **3**, **8**, and **9** exhibited 1.53-, 1.35-, and 1.20-fold improvements, respectively. These comparisons clearly demonstrate that the synthesized sulfaguanidine derivatives not only match but, in several cases, outperform currently marketed drugs, highlighting their promise as potent multitarget antidiabetic candidates.

The synthesized sulfaguanidine derivatives exhibited α-glucosidase IC_{50} values in the range of 0.39 to 1.61 μM and α-amylase IC_{50} values in the range of 0.33 to 1.33 μM. Interestingly, all the synthesized sulfaguanidine derivatives exhibited significant α-glucosidase and α-amylase inhibitory potentials that were more potent than acarbose. Additionally, the synthesized sulfaguanidine derivatives demonstrated an increase in glucose uptake with increased concentrations, revealing that the synthesized compounds in this study display substantial multitarget antidiabetic potential. Akocak *et al.*[21] reported the synthesis of substituted phenylureido sulfaguanidine derivatives, with α-glycosidase inhibition (IC_{50} values in the range of 0.094–0.40 μM). In another study, Işık *et al.*[31] synthesized thiadiazole-containing sulfonamide hybrids that inhibited α-glucosidase with IC_{50} values of 0.40–0.68 μM, indicating that sulfaguanidine derivative **10** (IC_{50} = 0.39 μM) surpassed the inhibitory activities of all similar scaffolds that were reported in their study. While these studies do not report dual-enzyme inhibition, our dual-activity data (both enzymes under one scaffold) offer a more convincing illustration of the adaptability of the sulfaguanidine core.

Thabet *et al.*[22] reported the synthesis of new hybrids of paracetamol and several sulfonamides to be screened for *in vitro* α-amylase and α-glucosidase activities. The most active diazo-paracetamol sulfa hybrids displayed IC_{50} values of 0.98 μM (α-amylase) and 1.39 μM (α-glucosidase), which are 3 and 3.5-fold less potent than those of our most active compounds **4** and **10** (IC_{50} = 0.33 μM and 0.39 μM, respectively).

Collectively, these comparisons demonstrate that our sulfaguanidine derivatives have superior dual-enzyme inhibition. Several compounds, in particular compounds **4** and **10**, outperform both structurally related inhibitors reported in recent literature and the reference drug acarbose (IC_{50} = 1.72 μM and 2.90 μM, against α-amylase and α-glucosidase, respectively). The significant increase in potency demonstrates the efficacy of the molecular hybridization approach used and the substantial contribution of this work to the development of strong multitarget antidiabetic drugs.

2.6. Molecular docking study

Molecular docking serves as a computational tool to predict and visualize how synthesized compounds interact with the target. It provides insights into binding modes, key interactions, and the potential efficacy of drug candidates, guiding further drug development. In this study, docking simulations were conducted on all synthesized compounds using the MOE software (version 2022.09).[32] The target enzymes were α-glucosidase (PDB ID: 2QMJ)[33] and α-amylase (PDB ID: 1XCW),[34] both co-crystallized with the known inhibitor acarbose.

The docking protocol was validated by re-docking acarbose into the active site of α-glucosidase, successfully reproducing the binding pose of the co-crystallized ligand acarbose, with an acceptable RMSD value within the cutoff threshold (RMSD = 0.76 Å), indicating the reliability of the docking method (SI). Structurally, acarbose comprises a maltose and an acarviosin moiety, of which the latter penetrates deeply into the α-glucosidase active site and mediates critical interactions with residues Arg526, Met444, His600, Asp203, and Asp542. The same protocol was then applied to the synthesized compounds to evaluate their binding profiles within the active site of human α-glucosidase (PDB: 2QMJ). As summarized in Table 2, several of the docked compounds occupied similar binding regions as the acarviosin portion of acarbose and displayed notable interactions with key active site residues. Interestingly, compounds **3**, **5**, **6**, **10**, and **11** emerged as the most active in the enzymatic inhibition assay and demonstrated notable docking interactions that paralleled those of acarbose. Compound **3** (Fig. 3) exhibited a docking score of −6.659 kcal mol^{-1} and the guanidine group formed multiple hydrogen bonds with Asp443, His600, and Asp542, in addition to stabilizing arene-H interactions with Trp406. Similarly, compound **5** (−6.4 kcal mol^{-1}) interacted through hydrogen bonds with Asp443, Asp327, and

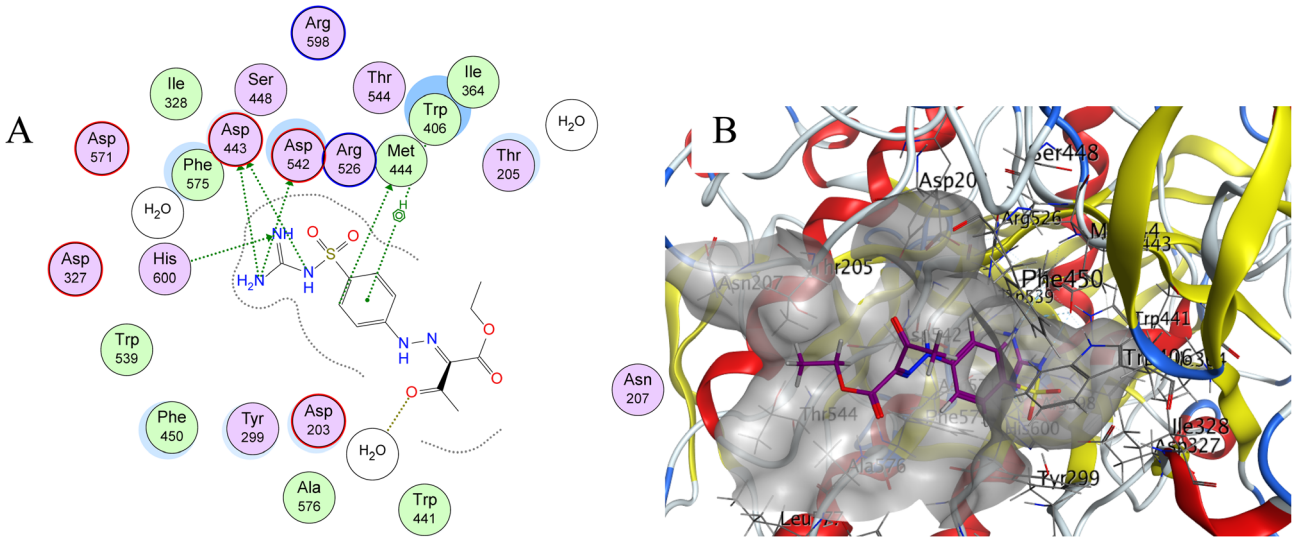

Fig. 3 A diagram showing (A) 2-D representation and (B) 3-D representation of molecular docking of compound **3** (magenta) in the α-glucosidase binding pocket (PDB: 2QMJ).

Met444, while also showing arene-H contacts with Trp406 and Phe450, highlighting its capacity to mimic acarbose's anchoring in the active site.

Compound **6** (Fig. 4), with a docking score of −6.22 kcal-mol^{-1}, displayed a nearly identical interaction pattern, forming hydrogen bonds with Asp443, Asp327, and Met444, as well as arene-H interactions with Trp406 and Phe450. An analysis of the enzyme inhibition profiles revealed that the synthesized compounds generally exhibited potent inhibitory activity against both α-glucosidase and α-amylase within the low micromolar range. While some variation in potency between the two enzymes was observed for individual compounds (*e.g.*, **4**, **5**, **7**, **10**, and **12**), the most notable trend across the series was a consistent enhancement of α-glucosidase inhibition relative to acarbose, indicating a preferential affinity of the scaffold for the α-glucosidase active site.

Molecular docking simulations provide a structural rationale for this trend. The common sulfaguanidine-pyrazole core consistently formed hydrogen bonds with key catalytic residues in α-glucosidase (Asp443, His600, and Asp542). Subtle differences in the aryl substituents on the pyrazole ring modulated these interactions; for example, the *para*-methylphenyl group in **10** facilitated additional stabilizing contacts. Although the compounds also docked favorably into the α-amylase active site, engaging residues such as His201 and Glu233, slight variations in ligand orientation and steric accommodation may explain the observed differences in inhibitory potency. Overall, these findings indicate that the synthesized compounds well-adapted for dual inhibition, with a particular preference for α-glucosidase, consistent with the IC_{50} results.

Compound **10** was among the top-scoring derivatives (−6.872 kcal mol^{-1}), forming strong hydrogen bonds of the

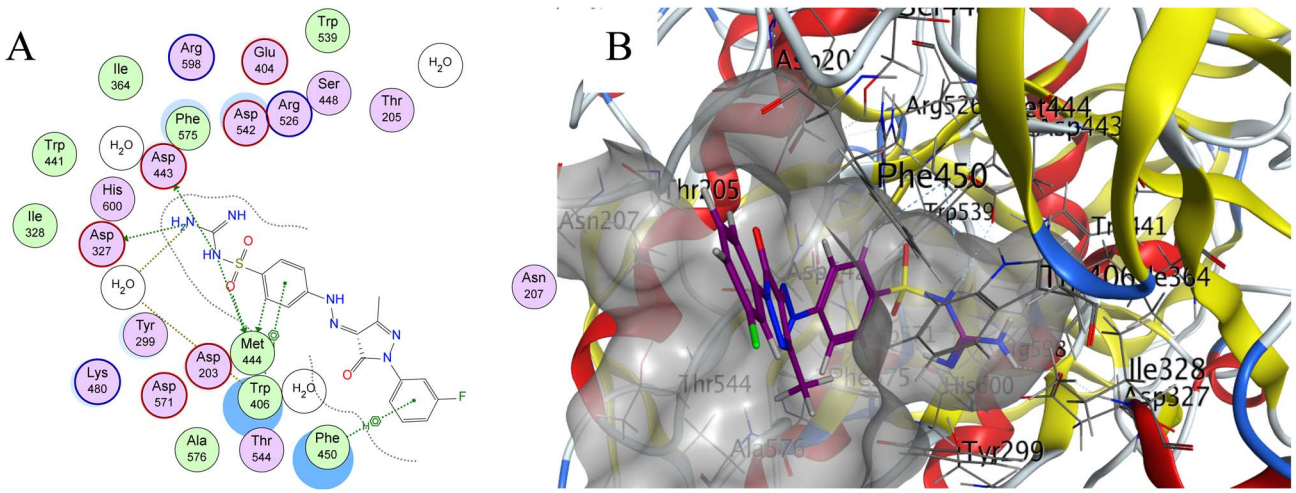

Fig. 4 A diagram showing (A) 2-D representation and (B) 3-D representation of molecular docking of compound **6** (magenta) in the α-glucosidase binding pocket (PDB: 2QMJ).

sulfaguanidine with Trp406, His600, and Met444 and engaging in arene-H interactions with Phe575, suggesting tight binding and proper positioning in the catalytic site. Likewise, compound **11** (−6.454 kcal mol^{-1}) maintained crucial hydrogen bonding interactions with Asp327, Met444, and His600, comparable to the binding pattern observed for acarbose. Overall, these docking results suggest that sulfaguanidine moiety is a key structural feature contributing to enhanced binding affinity and favorable interactions within the active site of α-glucosidase. Its inclusion improves hydrogen bonding potential and provides stabilizing interactions that are critical for effective enzyme inhibition. The docking results also highlight the importance of the key amino acid His600 interaction-n in increasing the activity, and the lack of the phenyl ring attached to the pyrazolone or the presence of *p*-chloro phenyl, as in compounds **7**,**12**, and **13**, may orient the sulfaguanidine group away from His600 leading to the loss of this crucial interaction that might lead to a decrease in the activity. These findings align with the experimental activity results and support further optimization of sulfaguanidine-containing scaffolds in the development of potent α-glucosidase inhibitors.

The docking of the compounds to α-amylase (PDB ID: 1XCW) highlights the key structural features shared by most promising compounds, which is the sulfaguanidine moiety, which contributes to strong hydrogen bonding, particularly with His299 and Asp300, residues essential for catalytic activity in α-amylase. In addition to the sulfaguanidine group, the pyrazolone ring system contributes significantly to binding strength and specificity. The pyrazolone scaffold interacts prominently with His201 and Ile235, stabilizing the ligand within the active site through hydrogen bonds and π–π stacking interactions (Fig. 5). This dual contribution of sulfaguanidine for polar interactions and pyrazolone for aromatic stacking underscores the synergistic effect of these moieties in achieving potent enzyme inhibition. The incorporation of an additional hydrophobic aromatic ring onto the pyrazole ring enhanced anchoring to the binding site through a stabilizing Arene–H interaction with Ala307. Consequently, lacking this hydrophobic aromatic ring as in compounds **12** and **13** represents a structural disadvantage as the loss of these key contacts results in their notably reduced inhibitory activity. Full docking poses and 2D interaction diagrams are available in SI. In conclusion, a clear agreement exists between the *in vitro* enzyme inhibition results and the docking findings. Compounds **3**, **6**, **10**, and **11** showed both strong docking scores and high inhibitory activity, which supports the reliability of the docking predictions. This activity is structurally rationalized by the sulfaguanidine group, which formed stable hydrogen bonds with key amino acids such as His600, Asp443, and Met444 in α-glucosidase and His299 and Asp300 in α-amylase. In contrast, compounds **7**, **12**, and **13** lacked some of these important interactions and showed lower activity. These results suggest that the computational data are consistent with the experimental outcomes and help explain why certain structural features enhance the inhibitory effect.

2.7. Prediction of physicochemical, pharmacokinetic, and ADME properties

To further evaluate the synthesized compounds, their physicochemical and ADME properties were predicted using SwissADME, an online platform for pharmacokinetic profiling.[35] The assessment included Lipinski's rule of five.[36] All compounds met the requirement in which at least three out of the four criteria indicate drug-likeness. All compounds showed a predicted low gastrointestinal (GI) absorption and generally low potential to cross the blood–brain barrier[37] (SI). A low gastrointestinal (GI) absorption is advantageous for these α-amylase and α-glucosidase inhibitors, as these enzymes primarily act within the intestinal lumen rather than in systemic circulation. Inhibitors with limited GI absorption will ensure that these drugs remain localized in the gut, allowing them to effectively interact with their enzymatic targets, which minimizes systemic exposure and reduces the risk of off-target effects or toxicity.

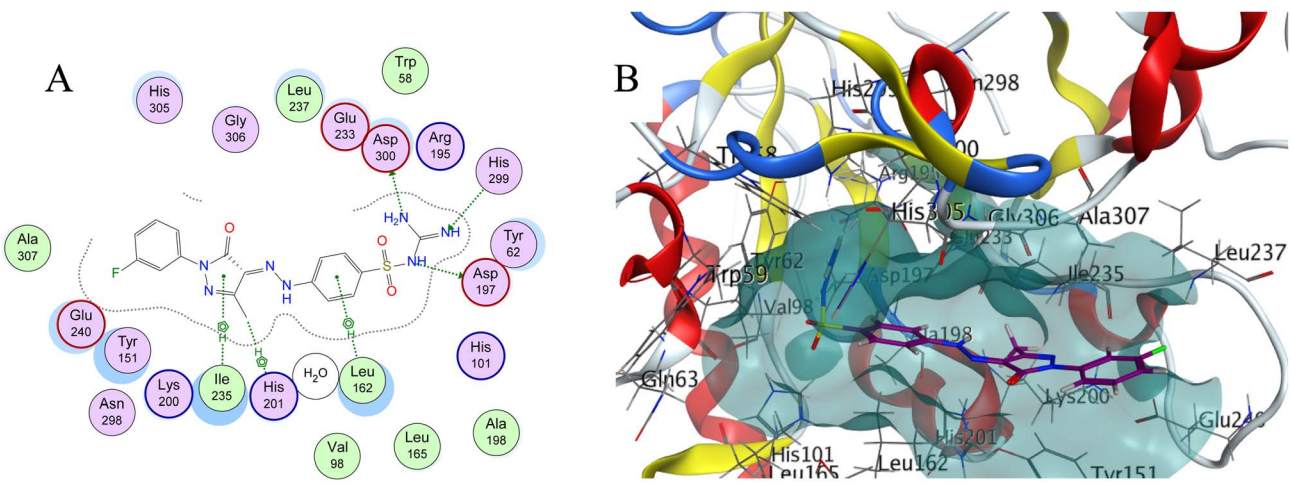

Fig. 5 A diagram showing (A) 2-D representation and (B) 3-D representation of molecular docking of compound **6** (magenta) in the α-amylase binding pocket (PDB:1XCW).

3. Conclusion

In summary, several novel sulfaguanidine derivatives with hydrazine-linked five-membered heterocycles were successfully designed, synthesized, and characterized in this study. According to the *in vitro* biological assessments, the synthesized compounds demonstrated notable inhibitory potentials against α-glucosidase and α-amylase, with several derivatives showing higher activity than the reference drug acarbose. Furthermore, several compounds enhanced glucose uptake activity compared to berberine. The strong *in vitro* inhibitory activity of the synthesized sulfaguanidine derivatives against both enzymes may be computationally explained by their considerable interactions with the α-amylase and α-glucosidase active sites. The results highlight the potential of pyrazole and oxazole scaffolds based on sulfaguanidine as prospective multitarget drug candidates for the treatment of type 2 diabetes mellitus. Aqueous solubility remains a critical parameter for their further pharmacological development. Experimental solubility measurements were not conducted in the present study; however, *in silico* physicochemical and ADME predictions indicated that the compounds generally possess high polarity and multiple hydrogen-bonding functionalities, which may partially mitigate solubility limitations. Nonetheless, comprehensive experimental solubility profiling, along with formulation optimization strategies, will be essential in future studies to fully assess the developability of these compounds. However, since the current findings are based solely on *in vitro* assays and computational analyses, more structure–activity relationship analysis and *in vivo* studies are necessary to validate their therapeutic potential and safety profiles. Such studies are essential for confirming and refining the synthesized sulfaguanidine derivatives as therapeutic candidates.

4. Experimental

4.1. Chemistry

4.1.1. Materials and methods. Unless otherwise stated, all chemicals and solvents were purchased from Sigma-Aldrich (Merck), were of analytical grade (≥98% purity), and were used as received without further purification. All reactions were carried out in dried glassware. NMR spectra were measured using a JEOL JNM-ECX 500 spectrometer. The deuterated solvent was used as an internal deuterium lock. ^{13}C NMR spectra were recorded using the UDEFT pulse sequence and broad-band proton decoupling at 125 MHz. All chemical shifts (δ) are stated in units of parts per million (ppm) and presented using TMS as the standard reference point. Melting points were obtained in open capillary tubes using Thermo Scientific, Model No. 1002D, 220–240 V; 200 W; 50/60 Hz. Samples were finely ground prior to measurement. Melting point ranges were recorded from the onset of melting (first visible liquefaction) to the clear point at which the sample was completely melted and are uncorrected. The reaction progress was monitored by TLC on Merck silica gel aluminum cards (0.2 mm thickness) with a fluorescent indicator at 254 nm. Visualization of the TLC during reaction monitoring was performed using a UV VILBER LOURMAT 4w-365 nm or 254 nm tube. Infrared (IR) spectra were recorded on a PerkinElmer 1600 series Fourier transform spectrometer using KBr pellets prepared from spectroscopic-grade KBr that had been thoroughly dried and stored in a sealed desiccator to prevent moisture uptake. Absorption bands ($\bar{\nu}_{max}$) are reported in wavenumbers (cm^{-1}). High-resolution mass spectra (HRMS) were recorded using an LC/Q-TOF 6530 mass spectrometer (Agilent Technologies, Santa Clara, CA, USA) equipped with an electrospray ionization (ESI) source and operated in negative ion mode at the Natural Product Research Laboratory, Fayoum University. Accurate mass measurements are reported as mass-to-charge ratios (m/z).

4.1.2. Procedure for the preparation of ethyl (*E*)-2-(2-(4-(*N*-carbamimidoylsulfamoyl)- phenyl)hydrazono)-3-oxobutanoate (3).[38] A solution of sodium nitrite (1.5 mmol, 1.5 equiv.) in 10 mL H_2O was added dropwise to a solution of sulfaguanidine (1.0 mmol, 1.0 equiv.) in AcOH (20 mL) and diluted with aq. HCl (5 mL) at 0 °C, the formed soluble diazonium salt solution was then added to a previously prepared solution from ethyl-acetoacetae (1.0 mmol, 1.0 equiv.) and AcONa (1.5 mmol, 1.5 equiv.) in ethanol (25 mL) and water (5 mL) at 0–5 °C. the reaction mixture was stirred for 4 hours, the precipitated solid was then filtered and recrystallized from ethanol to give **3** as a yellow powder (77%): m.p. = 190–191 °C; IR (KBr) ν_{max}/(cm^{-1}): 3464, 3415, 3364, 3328, and 3225 (NH and Guanidine group), 2979 (Csp3–H), and 1666 (C=N); ^{1}H NMR (500 MHz, DMSO-d_6) δ_H: 11.57 (s, 1H, N–**H**), 7.74 (d, J = 9.2 Hz, 2H, Ar–**H**), 7.50 (d, J = 8.4 Hz, 2H, Ar–**H**), 6.69 (bs, 4H, **H$_2$**NC(N**H**)N**H**SO$_2$), 4.32 (q, J = 6.9 Hz, 2H, CO(O)C**H$_2$**CH$_3$), 2.40 (s, 3H, COC**H$_3$**), 1.28 (t, J = 7.2 Hz, 3H, CO(O)CH$_2$C**H$_3$**) ppm. ^{13}C NMR (125 MHz, DMSO- d_6) δ_C: 193.8 (**C**OCH$_3$), 162.4 (**C**O(O)CH$_2$CH$_3$), 158.1, 144.7, 139.0, 133.0, 127.2, 114.7 (Ar–**C**), 61.3 (CO(O)**C**H$_2$CH$_3$), 25.3 (CO**C**H$_3$), 13.9 (CO(O)CH$_2$**C**H$_3$) ppm; Anal. Calcd. for $C_{13}H_{17}N_5O_5S$ (355.09): C, 43.94; H, 4.82; N, 19.71; S, 9.02; found: C, 43.81; H, 4.93; N, 19.57; S, 8.91. HRMS (ESI$^-$) m/z [M–H]$^-$ Cald for $C_{13}H_{16}N_5O_5S^-$: 354.08721 found: 354.08717.

4.1.3. General procedure for the preparation of compounds 4–13. To a solution of **3** (0.32 mmol, 1.0 equiv.) in 10 mL ethanol, (0.32 mmol, 1.0 equiv.) of arylhydrazine namely phenylhydrazine, *o*-fluorophenylhydrazine, *m*-fluorophenylhydrazine, *p*-chlorophenylhydrazine, *p*-nitrophenylhydrazine, 4-hydrazinobenzene sulfonamide, 2-pyridylhydrazine, and *p*-tolylhydrazine, was added for the synthesis of compounds **4–11** respectively or hydroxylamine or hydrazine hydrate for the synthesis of **13** or **14** respectively, the reaction mixture was heated near boiling point for 8 hours. The resulting solid was then filtered and crystallized from ethanol to afford the following compounds (**4–13**).

*4.1.3.1. (E)-N-Carbamimidoyl-4-(2-(3-methyl-5-oxo-1-phenyl-1H-pyrazol-4(5H)-ylidene)hydrazinyl)benzenesulfonamide (**4**).* Obtained as yellow powder (84%): m.p. = 253–255 °C; IR (KBr) ν_{max}/(cm^{-1}): 3430, 3339, and 3199 (NH and H$_2$NC(NH)NHSO$_2$), 2895 (Csp3–H), and 1629 (C=N); ^{1}H NMR (500 MHz, DMSO-d_6) δ_H: 13.21 (s, 1H, N–**H**), 7.90 (d, J = 7.6 Hz, 2H, Ar–**H**), 7.80 (d, J = 8.4 Hz, 2H, Ar–H), 7.70 (d, J = 8.4 Hz, 2H, Ar–H), 7.45 (t, J = 7.6 Hz, 2H, Ar–H), 7.22 (t, J = 7.2 Hz, 1H, Ar–H), 6.75 (s, 4H, **H$_2$**NC(N**H**)N**H**SO$_2$), 2.29 (s, 3H, –C**H$_3$**) ppm. ^{13}C NMR (125 MHz,

DMSO-d_6) δ_C: 158.1 (**C**=NH), 156.3 (**C**=O), 148.7, 143.5, 140.9, 137.8, 129.1, 127.2, 124.9, 117.7, 116.0 (Ar–C), 11.7 (–**C**H_3) ppm; Anal. Calcd. for $C_{17}H_{17}N_7O_3S$ (399.11): C, 51.12; H, 4.29; N, 24.55; S, 8.03; found: C, 51.28; H, 4.34; N, 24.64; S, 8.11. HRMS (ESI^-) m/z [M–H]$^-$ Cald for $C_{17}H_{16}N_7O_3S^-$: 398.10353 found: 398.10286.

*4.1.3.2. (E)-N-Carbamimidoyl-4-(2-(1-(2-fluorophenyl)-3-methyl-5-oxo-1H-pyrazol-4(5H)-ylidene)hydrazinyl)benzenesulfonamide (**5**).* Obtained as orange powder (71%): m.p. = 233–235 °C; IR (KBr) ν_{max}/(cm^{-1}): 3434, 3335, 3237 and 3106 (NH and $H_2NC(NH)NHSO_2$), 2894 (Csp3–H), and 1645 (C=N); ^{1}H NMR (500 MHz, DMSO-d_6) δ_H: 13.12 (s, 1H, N–**H**), 7.80 (d, J = 8.4 Hz, 2H, Ar–**H**), 7.70 (d, J = 8.4 Hz, 2H, Ar–**H**), 7.54 (t, J = 7.6 Hz, 1H, Ar–**H**), 7.49–7.40 (m, 2H, Ar–**H**), 7.33 (t, J = 7.6 Hz, 1H, Ar–**H**), 6.74 (bs, 4H, **H**$_2$NC(N**H**)N**H**SO_2), 2.28 (s, 3H, –C**H**$_3$) ppm. ^{13}C NMR (125 MHz, DMSO-d_6) δ_C: 158.1 (**C**=NH), 156.3 (**C**=O), 155.9 (d, $^1J_{C-F}$ = 249.5 Hz), 154.9, 149.0, 143.6, 141.0, 129.8 (d, $^3J_{C-F}$ = 7.9 Hz), 128.1, 127.4 (d, $^2J_{C-F}$ = 25.1 Hz), 125.0, 124.4 (d, $^3J_{C-F}$ = 11.9 Hz), 116.7 (d, $^2J_{C-F}$ = 19.3 Hz), 116.1 (Ar–C), 11.7 (**C**H_3) ppm; Anal. Calcd. for $C_{17}H_{16}FN_7O_3S$ (417.10): C, 48.92; H, 3.86; N, 23.49; S, 7.68; found: C, 48.75; H, 3.92; N, 23.31; S, 7.54. HRMS (ESI^-) m/z [M–H]$^-$ Cald for $C_{17}H_{15}FN_7O_3S^-$: 416.09411 found: 416.09279.

*4.1.3.3. (E)-N-Carbamimidoyl-4-(2-(1-(3-fluorophenyl)-3-methyl-5-oxo-1H-pyrazol-4(5H)-ylidene)hydrazinyl)benzenesulfonamide (**6**).* Obtained as orange powder (77%): m.p. = 239–241 °C; IR (KBr) ν_{max}/(cm^{-1}): 3570, 3434, 3347, and 3187 (NH and $H_2NC(NH)NHSO_2$), 2891 (Csp3–H), and 1623 (C=N); ^{1}H NMR (500 MHz, DMSO-d_6) δ_H: 13.16 (s, 1H, N–**H**), 7.80 (d, J = 8.4 Hz, 2H, Ar–**H**), 7.74 (d, J = 9.2 Hz, 2H, Ar–**H**), 7.69 (d, J = 8.4 Hz, 2H, Ar–**H**), 7.48 (q, J = 7.6 Hz, 1H, Ar–**H**), 7.03 (t, J = 8.8 Hz, 1H, Ar–**H**), 6.73 (bs, 4H, **H**$_2$NC(N**H**)N**H**SO_2), 2.28 (s, 3H, –C**H**$_3$) ppm. ^{13}C NMR (125 MHz, DMSO-d_6) δ_C: 162.2 (d, $^1J_{C-F}$ = 240.8 Hz), 158.1 (**C**=NH), 156.4 (**C**=O), 149.3, 143.5, 141.1, 139.3 (d, $^3J_{C-F}$ = 11.2 Hz), 131.0 (d, $^3J_{C-F}$ = 9.2 Hz), 128.8, 127.3, 116.2, 113.2, 111.4 (d, $^2J_{C-F}$ = 21.2 Hz), 104.3 (d, $^2J_{C-F}$ = 27.0 Hz), 11.7 (**C**H_3) ppm; Anal. Calcd. for $C_{17}H_{16}FN_7O_3S$ (417.10): C, 48.92; H, 3.86; N, 23.49; S, 7.68; found: C, 48.79; H, 3.96; N, 23.28; S, 7.51. HRMS (ESI^-) m/z [M–H]$^-$ Cald for $C_{17}H_{15}FN_7O_3S^-$: 416.09411 found: 416.09413.

4.1.3.4. (E)-N-Carbamimidoyl-4-(2-(1-(4-chlorophenyl)-3-methyl-5-oxo-1H-pyrazol-4(5H)-ylidene)hydrazinyl)benzenesulfonamide (7). Obtained as orange powder (88%): m.p. = 273–274 °C; IR (KBr) ν_{max}/(cm^{-1}): 3443, 3335, 3186, and 3134 (NH and $H_2NC(NH)NHSO_2$), 2829 (Csp3–H), and 1627 (C=N);^{1}H NMR (500 MHz, DMSO-d_6) δ_H: 13.16 (s, 1H, N–**H**), 7.91 (d, J = 9.0 Hz, 2H, Ar–**H**), 7.80 (d, J = 8.8 Hz, 2H, Ar–**H**), 7.69 (d, J = 8.8 Hz, 2H, Ar–**H**), 7.49 (d, J = 9.0 Hz, 2H, Ar–**H**), 6.74 (bs, 4H, **H**$_2$NC(N**H**)N**H**SO_2), 2.27 (s, 3H, –C**H**$_3$) ppm. ^{13}C NMR (125 MHz, DMSO-d_6) δ_C: 158.1 (**C**=NH), 156.2 (**C**=O), 149.1, 143.4, 141.0, 136.7, 129.0, 128.9, 128.7, 127.3, 119.1, 116.1 (Ar–C), 11.7 (–**C**H_3) ppm. Anal. Calcd. for $C_{17}H_{16}ClN_7O_3S$ (433.07): C, 47.06; H, 3.72; N, 22.60; S, 7.39; found: C, 47.06; H, 3.72; N, 22.60; S, 7.39. HRMS (ESI^-) m/z [M–H]$^-$ Cald for $C_{17}H_{15}ClN_7O_3S^-$: 432.06456 found: 432.06422.

*4.1.3.5. (E)-N-Carbamimidoyl-4-(2-(3-methyl-1-(4-nitrophenyl)-5-oxo-1H-pyrazol-4(5H)-ylidene)hydrazinyl)benzenesulfonamide (**8**).* Obtained as orange powder (67%): m.p. > 300 °C; IR (KBr) ν_{max}/(cm^{-1}): 3431, 3331, and 3208 (NH and $H_2NC(NH)NHSO_2$), 2893 (Csp3–H), and 1633 (C=N);^{1}H NMR (500 MHz, DMSO-d_6) δ_H: 13.13 (s, 1H, N–**H**), 8.33 (d, J = 9.2 Hz, 2H, Ar–**H**), 8.15 (d, J = 9.2 Hz, 2H, Ar–**H**), 7.81 (d, J = 9.2 Hz, 2H, Ar–**H**), 7.73 (d, J = 8.5 Hz, 2H, Ar–**H**), 6.73 (bs, 4H, **H**$_2$NC(N**H**)N**H**SO_2), 2.31 (s, 3H, –C**H**$_3$) ppm. ^{13}C NMR (125 MHz, DMSO-d_6) δ_C: 158.2 (**C**=NH), 156.8 (**C**=O), 150.6, 143.4, 143.2, 142.9, 141.3, 128.4, 127.3, 125.2, 117.1, 116.4 (Ar–C), 11.8 (–**C**H_3) ppm. Anal. Calcd. for $C_{17}H_{16}N_8O_5S$ (444.096): C, 45.94; H, 3.63; N, 25.21; S, 7.21; found: C, 45.70; H, 3.41; N, 25.35; S, 7.40. HRMS (ESI^-) m/z [M–H]$^-$ Cald for $C_{17}H_{15}N_8O_5S^-$: 443.08861 found: 443.08693.

*4.1.3.6. (E)-N-Carbamimidoyl-4-(2-(3-methyl-5-oxo-1-(4-sulfamoylphenyl)-1H-pyrazol-4(5H)-ylidene)hydrazinyl)benzenesulfonamide (**9**).* Obtained as pale yellow powder (62%): m.p. = 278–280 °C; IR (KBr) ν_{max}/(cm^{-1}): 3436, 3330, and 3204 (NH, SO_2**N**H_2 and $H_2NC(NH)NHSO_2$), 2983 (Csp3–H), 1675 (C=O), and 1627 (C=N);^{1}H NMR (500 MHz, DMSO-d_6) δ_H: 13.18 (s, 1H, N–**H**), 8.10 (d, J = 8.5 Hz, 2H, Ar–**H**), 7.91 (d, J = 8.5 Hz, 2H, Ar–**H**), 7.81 (d, J = 8.5 Hz, 2H, Ar–**H**), 7.72 (d, J = 8.5 Hz, 2H, Ar–**H**), 7.38 (s, 2H, SO_2N**H**$_2$), 6.74 (bs, 4H, **H**$_2$NC(N**H**)N**H**SO_2), 2.32 (s, 3H, **C**H_3) ppm. ^{13}C NMR (125 MHz, DMSO-d_6) δ_C:158.2 (**C**=NH), 156.7 (**C**=O), 149.8, 143.5, 141.1, 140.3, 139.8, 128.8, 127.3, 127.1, 117.2, 116.3 (Ar–C), 11.8 (–**C**H_3) ppm; Anal. Calcd. for $C_{17}H_{18}N_8O_5S_2$ (478.08): C, 42.67; H, 3.79; N, 23.42; S, 13.40; found: C, 42.76; H, 3.83; N, 23.51; S, 13.51. HRMS (ESI^-) m/z [M–H]$^-$ Cald for $C_{17}H_{17}N_8O_5S_2^-$: 477.07633 found: 477.07488.

*4.1.3.7. (E)-N-Carbamimidoyl-4-(2-(3-methyl-5-oxo-1-(p-tolyl)-1H-pyrazol-4(5H)-ylidene)hydrazinyl)benzenesulfonamide (**10**).* Obtained as orange powder (91%): m.p. = 268–270 °C; IR (KBr) ν_{max}/(cm^{-1}): 3433, 3336, and 3217 (NH and $H_2NC(NH)NHSO_2$), 2980 (Csp3–H), and 1629 (C=N);^{1}H NMR (500 MHz, DMSO-d_6) δ_H: 13.21 (s, 1H, N–**H**), 7.81–7.76 (m, 4H, Ar–**H**), 7.67 (d, J = 8.4 Hz, 2H, Ar–**H**), 7.23 (d, J = 8.4 Hz, 2H, Ar–**H**), 6.76 (s, 4H, **H**$_2$NC(N**H**)N**H**SO_2), 2.29 (s, 3H, –C**H**$_3$, attached to the phenyl ring), 2.26 (s, 3H, –C**H**$_3$, attached to the triazole ring) ppm. ^{13}C NMR (125 MHz, DMSO-d_6) δ_C: 158.1 (**C**=NH), 156.1 (**C**=O), 148.4, 143.4, 140.9, 135.4, 134.1, 129.4, 129.2, 127.2, 117.7, 115.9, (Ar–C), 20.5 (–**C**H_3, attached to the phenyl ring), 11.6 (–**C**H_3, attached to the triazole ring) ppm. Anal. Calcd. for $C_{18}H_{19}N_7O_3S$ (413.12): C, 52.29; H, 4.63; N, 23.71; S, 7.75; found: C, 52.42; H, 4.76; N, 23.69; S, 7.67. HRMS (ESI^-) m/z [M–H]$^-$ Cald for $C_{18}H_{18}N_7O_3S^-$: 412.11918 found: 412.11854.

*4.1.3.8. (E)-N-Carbamimidoyl-4-(2-(3-methyl-5-oxo-1-(pyridin-2-yl)-1H-pyrazol-4(5H)-ylidene)hydrazinyl)benzenesulfonamide (**11**).* Obtained as orange powder (63%): m.p. = 280–282 °C; IR (KBr) ν_{max}/(cm^{-1}): 3431, 3314, and 3116 (NH and $H_2NC(NH)NHSO_2$), 2832 (Csp3–H), and 1640 (C=N);^{1}H NMR (500 MHz, DMSO-d_6) δ_H: 13.15 (s, 1H, N–**H**), 8.47 (d, J = 4.9 Hz, 1H, ***ortho*-pyridyl-H$_a$**), 7.92 (td, J = 8.4, 1.9 Hz, 1H, ***para*-pyridyl-H$_c$**), 7.85 (d, J = 8.4 Hz, 1H, ***meta*-pyridyl-H$_d$**), 7.80 (d, J = 8.8 Hz, 2H, Ar–**H**), 7.69 (d, J = 8.8 Hz, 2H, Ar–**H**), 7.35–7.18 (m, 1H, ***meta*-pyridyl-H$_b$**), 6.76 (bs, 4H, **H**$_2$NC(N**H**)N**H**SO_2), 2.29 (s, 3H, –CH_3) ppm. ^{13}C NMR (125 MHz, DMSO-d_6) δ_C: 158.1 (**C**=NH), 156.6 (**C**=O), 149.4, 148.9, 148.5, 143.5, 140.9, 138.4, 128.7, 127.3, 121.2, 116.0, 113.9 (Ar–C), 11.7 (–**C**H_3) ppm. Anal. Calcd. for $C_{16}H_{16}N_8O_3S$ (478.08): C, 42.67; H, 3.79; N, 23.42; S, 13.40

found: C, 42.74; H, 3.85; N, 23.39; S, 13.36. HRMS (ESI$^-$) m/z [M–H]$^-$ Cald for $C_{16}H_{15}N_8O_3S^-$: 399.09878 found: 399.09844.

*4.1.3.9. (E)-N-Carbamimidoyl-4-(2-(3-methyl-5-oxoisoxazol-4(5H)-ylidene)hydrazinyl)benzenesulfonamide (**12**).* Obtained as orange powder (79%): m.p. = 216–218 °C; IR (KBr) ν_{max}/(cm^{-1}): 3442, 3348, 3319 and 3207 (NH and $H_2NC(NH)NHSO_2$), 2893 (Csp3–H), 1718 (C=O) and 1632 (C=N);^{1}H NMR (500 MHz, DMSO-d_6) δ_H: 12.77 (s, 1H, N–**H**), 7.79 (d, J = 8.5 Hz, 2H, Ar–**H**), 7.75 (d, J = 8.4 Hz, 2H, Ar–**H**), 6.72 (bs, 4H, $\mathbf{H_2}NC(N\mathbf{H})N\mathbf{H}SO_2$), 2.26 (s, 3H, –$\mathbf{C}H_3$) ppm. ^{13}C NMR (125 MHz, DMSO-d_6) δ_C: 162.1 (**C**=O), 160.1, 158.1 (**C**=NH), 143.5, 141.4, 127.1, 121.9, 116.7, 10.1 (–$\mathbf{C}H_3$) ppm. Anal. Calcd. for $C_{11}H_{12}N_6O_4S$ (324.06): C, 40.74; H, 3.73; N, 25.91; S, 9.89 found: C, 40.48; H, 3.90; N, 25.83; S, 9.72. HRMS (ESI$^-$) m/z [M–H]$^-$ Cald for $C_{11}H_{11}N_6O_4S^-$: 323.05625 found: 323.05634.

*4.1.3.10. (E)-N-Carbamimidoyl-4-(2-(3-methyl-5-oxo-1H-pyrazol-4(5H)-ylidene)hydrazinyl)benzenesulfonamide (**13**).* Obtained as orange powder (84%): m.p. = 262–264 °C; IR (KBr) ν_{max}/(cm^{-1}): 3446, 3417, 3310 and 3205 (NH and $H_2NC(NH)NHSO_2$), 2894 (Csp3–H), 1672 (C=O) and 1631 (C=N);^{11}H NMR (500 MHz, DMSO-d_6) δ_H: 11.61 (s, 1H, N–**H**), 7.76–7.49 (m, 2 overlapped doublets and N**H**-pyrazole, 5H), 6.70 (bs, 4H, $\mathbf{H_2}NC(N\mathbf{H})N\mathbf{H}SO_2$), 2.15 (s, 3H, –$\mathbf{C}H_3$) ppm. ^{13}C NMR (125 MHz, DMSO-d_6) δ_C: 160.0 (**C**=O), 158.1 (**C**=NH), 147.0, 143.6, 140.4, 129.5, 127.2, 115.4 (Ar–C), 11.6 (–$\mathbf{C}H_3$) ppm. Anal. Calcd. for $C_{11}H_{13}N_7O_3S$ (323.08): C, 40.86; H, 4.05; N, 30.32; S, 9.92 found: C, 40.75; H, 4.13; N, 30.24; S, 9.80. HRMS (ESI$^-$) m/z [M–H]$^-$ Cald for $C_{11}H_{12}N_7O_3S^-$: 322.07223 found: 322.07174.

4.2. Biological evaluation

The biological α-glucosidase inhibitory assay,[39] α-amylase inhibitory assay,[40] and glucose uptake assay[30,41] were conducted following previously published protocols and are included in the SI.

4.3. Docking studies

The crystal structures of α-glucosidase (PDB ID: 2QMJ, 1.90 Å resolution) and α-amylase (PDB ID: 1XCW, 2.00 Å resolution) were retrieved from the Protein Data Bank (https://www.rcsb.org/). Molecular modeling and docking experiments were performed using MOE 2022.09 (Chemical Computing Group, Canada). Before docking, hydrogen atoms were added, and protonation states of amino acid residues were assigned using the Protonate 3D algorithm, followed by the addition of atomic partial charges. The test compounds were sketched with the MOE Builder tool and energy-minimized using the MMFF94× force field. Docking was carried out with the MOE Induced-Fit Dock protocol to accommodate ligand flexibility within the enzyme binding pocket. The final ligand–enzyme complexes were selected based on their binding energy scores in conjunction with favorable ligand–receptor interactions.

Conflicts of interest

There are no conflicts to declare.

Data availability

The data supporting this article have been included either in the main text or as part of the supplementary information (SI). Supplementary information: full synthetic characterization (^{1}H/^{13}C NMR, IR, HRMS), detailed biological assay procedures, and molecular docking diagrams for all compounds (2D/3D poses in PDB: 2QMJ). See DOI: https://doi.org/10.1039/d5ra08959j.

Funding

This work was supported by "the Deanship of Scientific Research, Vice Presidency for Graduate Studies and Scientific Research, King Faisal University, Saudi Arabia [Project No. KFU260108]".

Acknowledgements

MSA acknowledges "the Deanship of Scientific Research, Vice Presidency for Graduate Studies and Scientific Research, King Faisal University, Saudi Arabia, for financial support under the annual funding track [KFU260108]".

References

1 M. Lotfy, J. Adeghate, H. Kalasz, J. Singh and E. Adeghate, *Curr. Diabetes Rev.*, 2017, **13**, 3–10.
2 S. Chatterjee, K. Khunti and M. J. Davies, *Lancet*, 2017, **389**, 2239–2251.
3 D. Magliano, E. Boyko and I. Atlas, *"COVID-19 and Diabetes," IDF DIABETES ATLAS*, International Diabetes Federation, 10th edn, 2021.
4 K. Esposito, M. Ciotola, M. I. Maiorino and D. Giugliano, *Curr. Atheroscler. Rep.*, 2008, **10**, 523–528.
5 Y. Wu, Y. Ding, Y. Tanaka and W. Zhang, *Int. J. Med. Sci.*, 2014, **11**, 1185.
6 S. Wild, G. Roglic, A. Green, R. Sicree and H. King, *Diabetes Care*, 2004, **27**, 1047–1053.
7 M. J. Weigensberg and M. I. Goran, *Lancet*, 2009, **373**, 1743–1744.
8 Š. Janeček, B. Svensson and E. A. MacGregor, *Cell. Mol. Life Sci.*, 2014, **71**, 1149–1170.
9 Y. Chen, Y. Xiao, G. Lian, J. Yi and X. Liu, *Expert Opin. Drug Saf.*, 2023, 1–10.
10 E. C. Ebert, *Disease-a-Month*, 2005, **51**, 620–663.
11 R. V. Kumar and V. R. Sinha, *Expert Opin. Drug Delivery*, 2012, **9**, 403–416.
12 H. S. Yee and N. T. Fong, *Pharmacotherapy*, 1996, **16**, 792–805.
13 M. K. Moon, K.-Y. Hur, S.-H. Ko, S.-O. Park, B.-W. Lee, J. H. Kim, S. Y. Rhee, H. J. Kim, K. M. Choi and N.-H. Kim, *Diabetes metab. j.*, 2017, **41**, 357.
14 S. Bolen, L. Feldman, J. Vassy, L. Wilson, H.-C. Yeh, S. Marinopoulos, C. Wiley, E. Selvin, R. Wilson and E. B. Bass, *Ann. Intern. Med.*, 2007, **147**, 386–399.

15 C. J. Bailey and R. C. Turner, *N. Engl. J. Med.*, 1996, **334**, 574–579.
16 L. Yao, L. Wang, R. Zhang, A. A. Soukas and L. Wu, *TEM (Trends Endocrinol. Metab.)*, 2025, **36**, 364–372.
17 D. L. Wilansky, I. Hahn and R. Schucher, *Metabolism*, 1965, **14**, 793–799.
18 D. Sola, L. Rossi, G. P. C. Schianca, P. Maffioli, M. Bigliocca, R. Mella, F. Corlianò, G. P. Fra, E. Bartoli and G. Derosa, *Arch. Med. Sci.*, 2015, **11**, 840–848.
19 H. Ullah, N. Nadeem, F. Rahim, A. Nawaz and A. Hussain, *Chem. Data Collect.*, 2023, **46**, 101047.
20 M. S. Ayoup, N. Khaled, H. Abdel-Hamid, D. A. Ghareeb, S. A. Nasr, A. Omer, A. Sonousi, A. E. Kassab and A. S. Eltaweil, *RSC Adv.*, 2024, **14**, 7664–7675.
21 S. Akocak, P. Taslimi, N. Lolak, M. Işık, M. Durgun, Y. Budak, C. Türkeş, İ. Gülçin and Ş. Beydemir, *Chem. Biodiversity*, 2021, **18**, e2000958.
22 H. K. Thabet, A. Ragab, M. Imran, M. H. Helal, S. I. Alaqel, A. Alshehri, A. A. Mohd, M. R. Alshammari, M. S. Abusaif and Y. A. Ammar, *Eur. J. Med. Chem.*, 2024, **275**, 116589.
23 P. de Sena Murteira Pinheiro, L. S. Franco, T. L. Montagnoli and C. A. M. Fraga, *Expert Opin. Drug Discovery*, 2024, **19**, 451–470.
24 G. Ahmad, M. Sohail, M. Bilal, N. Rasool, M. U. Qamar, C. Ciurea, L. G. Marceanu and C. Misarca, *Molecules*, 2024, **29**, 2232.
25 S. Galiè, M. A. Fouad, C. Abbo, F. Ferretti and F. Ragaini, *Asian J. Org. Chem.*, 2025, e00555.
26 N. Sivaraj, K. Sakthivel, K. Kikushima, M. D. Kostić, T. Dohi and F. V. Singh, *RSC Adv.*, 2025, **15**, 35509–35531.
27 F. Ragaini, F. Ferretti and M. A. Fouad, *Catalysts*, 2023, **13**, 224.
28 A. Widauer, T. L. Petrick and D. E. Braun, *Cryst. Growth Des.*, 2024, **24**, 1438–1457.
29 A. N. Muttathukattil, S. Srinivasan, A. Halder and G. Reddy, *J. Phys. Chem. B*, 2019, **123**, 9302–9311.
30 V. P. Cirillo, *J. Bacteriol.*, 1962, **84**, 485–491.
31 M. Işık, S. Akocak, N. Lolak, P. Taslimi, C. Türkeş, İ. Gülçin, M. Durgun and Ş. Beydemir, *Arch. Pharm.*, 2020, **353**, 2000102.
32 C. ULC, *Molecular Operating Environment (MOE), 2020.09, Chemical Computing Group ULC*, McGill University, Montreal, QC, Canada, 2020.
33 L. Sim, R. Quezada-Calvillo, E. E. Sterchi, B. L. Nichols and D. R. Rose, *J. Mol. Biol.*, 2008, **375**, 782–792.
34 C. Li, A. Begum, S. Numao, K. H. Park, S. G. Withers and G. D. Brayer, *Biochemistry*, 2005, **44**, 3347–3357.
35 A. Daina, O. Michielin and V. Zoete, *Sci. Rep.*, 2017, **7**, 42717.
36 C. A. Lipinski, *Drug Discovery Today:Technol.*, 2004, **1**, 337–341.
37 A. Daina and V. Zoete, *ChemMedChem*, 2016, **11**, 1117–1121.
38 E. M. Husseiny, H. S. Abulkhair, S. A. El-Sebaey, M. M. Sayed and K. E. Anwer, *Future Med. Chem.*, 2024, **16**, 2487–2505.
39 T. Matsui, C. Yoshimoto, K. Osajima, T. Oki and Y. Osajima, *Biosci., Biotechnol., Biochem.*, 1996, **60**, 2019–2022.
40 V. K. Kumar and K. Lalitha, *Indian J. Pharmacol.*, 2014, **46**, 350–351.
41 V. S. Madiwalar, P. S. Dwivedi, A. Patil, S. M. Gaonkar, V. J. Kumbhar, P. Khanal and B. Patil, *J. Diabetes Metab. Disord.*, 2022, **21**, 429–438.